J Mater Sci (2006) 41:8284–8294
DOI 10.1007/s10853-006-1008-5

Viscoelastic properties of hybrid copolymers based on methacryloxypropyl-grafted nanosilica and methyl methacrylate

M. Mauger · A. Dubault · J. L. Halary

Received: 20 February 2004 / Accepted: 24 October 2005 / Published online: 14 November 2006

Abstract The linear viscoelastic behavior of ''model'' hybrid materials based on methyl methacrylate and methacryloxypropyl-grafted nanosilica was investigated. As unique features, the materials under study present an excellent dispersion of silica within the polymer matrix and are almost free of uncross-linked chains. In addition, very progressive changes in network architecture are available, resulting from changes in particle diameter, d, volume fraction of filler, Φ, number of methacryloyl units grafted per surface unit of silica particle, n, and nature of the grafting agent. The influence of these parameters on the characteristics of the mechanically active relaxations α and β was examined. Emphasis was put on the storage modulus, E', on the loss modulus, E'', and on their dependence on filler volume fraction. E'' values were shown to simply account for the reduction of the mechanical energy lost within the material, in connection to the occurrence of polymer molecular motions. Analysis of E' variations as a function of Φ was based on the theoretical models available in the literature to account for the contribution of the spherical filler particles. In the glassy state, Kerner's and Christensen and Lo's models yielded comparable results. In the rubbery state, Guth and Gold's model was shown to prevail on Kerner's model.

M. Mauger · A. Dubault · J. L.Halary (✉)
Laboratoire PPMD (UMR 7615), Ecole Supérieure de Physique et Chimie Industrielles de la Ville de Paris, 10, rue Vauquelin, 75231 Paris cedex 05, France
e-mail: jean-louis.halary@espci.fr

Introduction

Elaboration of organic–inorganic nanocomposites has experienced a growing interest in the last decade [1]. By contrast to micrometer-sized particles, which have been incorporated routinely in the industrial formulation of thermoplastics, nanometer-sized fillers are expected to improve performance at quite very low particle concentration. Indeed, the interaction of the polymer chains with the surface of inorganic particles is dramatically increased with decreasing particle size at same volume fraction. Additional improvements may also result from changes in the interaction strength coming from changes in chemical structure of both polymer and filler. Not only the improvement of mechanical behavior [2, 3] is concerned, but also various properties including reduced gas permeability [4], increased solvent resistance [5], reduced flammability [6, 7], increased thermal stability [8].

Among the thermoplastic polymers, PMMA has concentrated some attention, specially in the perspective of producing transparent coatings of improved surface hardness and scratch resistance. Reports concern different type of fillers, namely silica [9], clay particles [10, 11] and even alumina [12, 13].

The present paper reports on the viscoelastic behavior of hybrid organic–inorganic materials, based on nanosilica particles first grafted in surface by 3-methacryloxypropyl (MOP) units, then dispersed in a methyl methacrylate matrix, and finally copolymerized. Two series of samples were prepared by changing the nature of the grafting agent bearing the MOP units: either 3-(trimethoxysilyl) propyl methacrylate (referred to as MTOS):

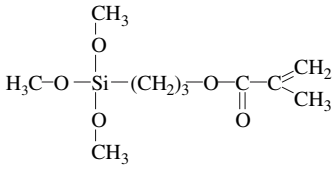

or 3-(chlorodimethylsilyl) propyl methacrylate (referred to as MDCS):

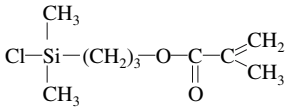

Copolymerization of the grafted chains with MMA leads to tri-dimensional networks, in which the inorganic nanosilica particles play the role of cross-links. As shown in Fig. 1, details of the network architecture depend of the choice of the grafting agent. Different network architectures have been obtained by varying the particle diameter, d, the volume fraction of filler, Φ, the number of 3-methacryloxypropyl units grafted per surface unit of particle, n. The synthesis route to highly transparent materials via a homogeneous dispersion of particles in the thermoplastic matrix is detailed elsewhere [9]. Quality of particle dispersion is shown in Fig. 2. The physico-chemical properties (swelling behavior, glass transition temperature) of the whole synthesized materials have shown that the network architecture could be characterized by a unique parameter, namely ξ_D, defined as the number of grafting agent double bonds per unit volume of polymer matrix:

$$\xi_D = \frac{6n\Phi}{(1-\Phi)d}$$

This parameter ξ_D accounts for the cross-link density: the higher the ξ_D value, the larger the cross-link density.

Experimental

Samples

The samples have been prepared according to the synthesis route detailed in reference [9] and adapted from the procedure originally reported by Ford and coworkers [14–17].

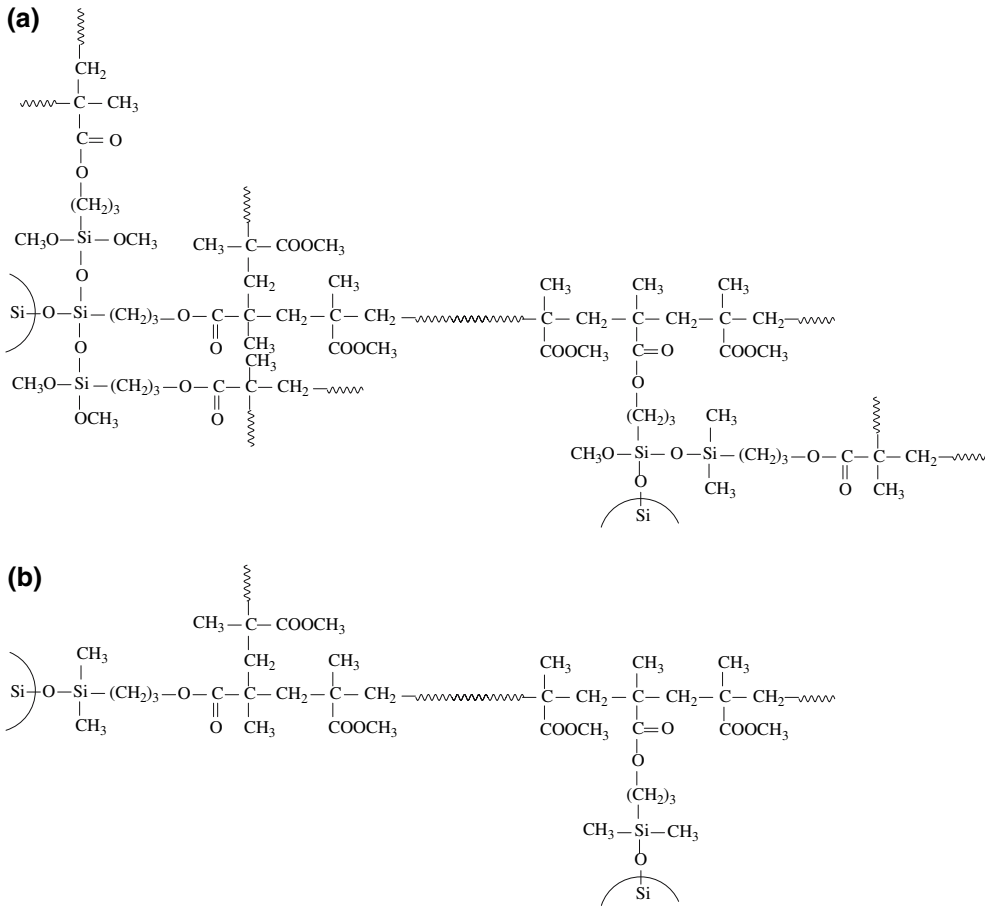

Fig. 1 Scheme for the grafting of (**a**) MTOS, and (**b**) MDCS onto the surfaces of silica particles

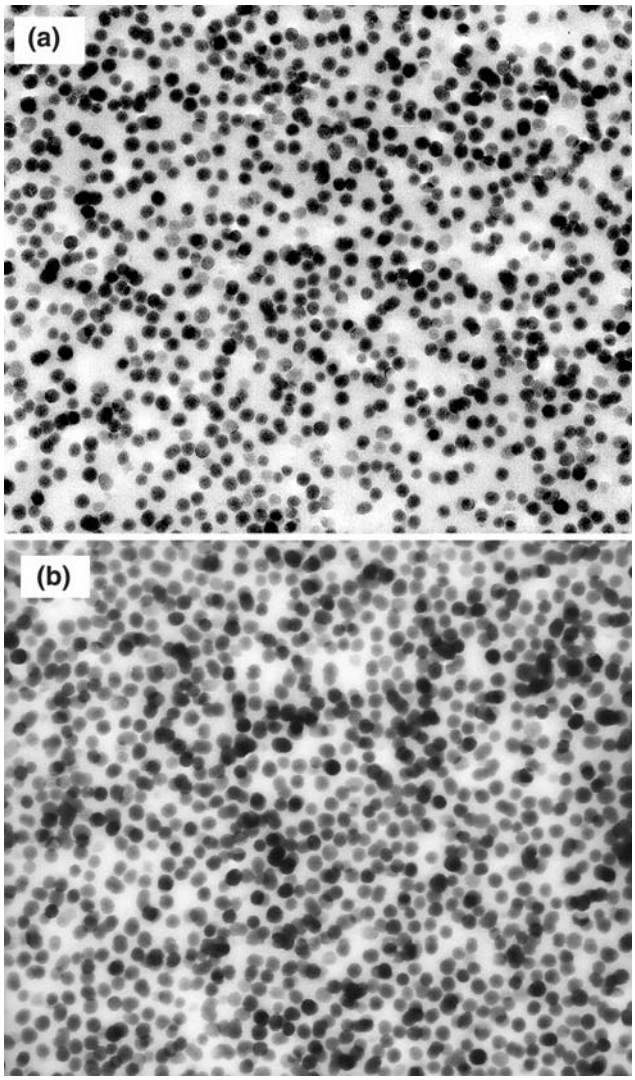

Fig. 2 Examples of transmission electron micrographs of the hybrids (**a**) MTOS d = 50 nm, Φ = 0.20. (**b**) MDCS d = 60 nm, Φ = 0.20

Spherical particles of ''Stöber silica'' were produced by the hydrolysis of tetraethoxysilane in ethanol in the presence of calculated amounts of water and ammonia. The MTOS grafting was carried out directly in the Stöber medium, for 12 h under continuous stirring. Then, the grafted silica dispersion was first transferred to methanol and then to the MMA monomer by successive dialysis. The silica particle concentration was adjusted to the desired volume fraction, ϕ. In the case of MDCS, the ''Stöber solvents'' were first exchanged with propylene carbonate by dialysis, and then the MDCS grafting was carried out in propylene carbonate for 12 h under stirring. Finally, the grafted dispersion was transferred, as above, to the MMA monomer by dialysis.

Table 1 Values of T_α (measured at 1 Hz) and T_g (measured at 10 K mn^{-1})

Sample reference	$T_\alpha \pm 2$ (°C)	$T_g \pm 2$ (°C)
PMMA	118	119
MTOS/30/0.11/7/0.17	120	121
MTOS/50/0.06/18.2/0.14	118	119
MTOS/50/0.10/18.2/0.24	121	123
MTOS/55/0.18/7.3/0.17	123	124
MTOS/55/0.21/11/0.32	133	130
MTOS/100/0.21/18.5/0.30	125	128
MTOS/100/0.09/23.5/0.14	124	127
MTOS/100/0.19/23.5/0.33	130	128
MDCS/30/0.16/2.8/0.11	111	111
MDCS/30/0.11/1.9/0.05	121	120
MDCS/30/0.13/2.6/0.08	118	122

A great number of samples were synthesized and characterized. However, the viscoelastic measurements have been undertaken only on those materials whose substantial amount of tri-dimensional character has been ascertained by the absence of extractible material during swelling experiments [9]. In the case of MTOS agent, only materials exhibiting a gel fraction higher than 0.95 have been mechanically tested. In fact, this criterion can be satisfied by simultaneously changing the parameters d, Φ and n taken into account in ξ_D; thus, the condition $\xi_D > 0.12$ is equivalent to the criterion on gel fraction. As it has been ascertained [9] that the use of MDCS agent led to less dense networks, we have chosen a less drastic criterion in that case: all selected MDCS materials have a gel fraction higher than 0.85, i.e., $\xi_D > 0.05$.

The materials are coded by using the following nomenclature: Grafting agent (MTOS or MDCS)/d (nm)/Φ/n/ξ_D.

The references of the tested materials appear in the first column of Table 1. Depending on the samples, the silica particle diameter, d, covered the range 30–100 nm; the silica volume fraction, Φ, ranged from 0.06 to 0.21; the silica grafting density (bonds/nm^2), n, varied from 1.9 to 2.8 in the MDCS series and from 7 to 23.5 in the MTOS series for which both direct and indirect grafting are likely to occur. Thus, the overall range of ξ_D covered was 0.05–0.33.

Viscoelastic measurements

All samples have been tested according to the same experimental procedure. Measurements were performed on a servo-hydraulic testing system MTS 831 operated in tensile mode. A routine available on the testing system allowed automatic calculation of: (a) the two components of the complex modulus E^*, namely

the storage modulus, E', and the loss modulus, E'', (b) tan $\delta = E''/E'$ and (c) the storage compliance $J' = \frac{E'}{E'^2+E''^2}$ and the loss compliance $J'' = \frac{E''}{E'^2+E''^2}$.

The sample size was 3*15*40 mm^3. Each sample was subjected to a static tensile strain of 0.1% on which a sinusoidal strain of ±0.05% was superimposed. In these conditions, the sample is always tested in traction and deformation is sufficiently small so that linear viscoelasticity conditions are fulfilled. Experiments were performed at 1 Hz for temperatures ranging from –40 °C to 160 °C. The temperature gap between two successive measurements was, respectively equal to 4 K in the low temperature range and 2 K near the main relaxation temperature, T_α, conventionally defined as the maximum of the loss modulus E'' in the glass transition region. Prior to the mechanical test, each sample was annealed for 15 h at a temperature 10 K above the glass transition temperature T_g, in order to erase the residual stresses. Then, any physical aging of the materials was avoided by fast cooling below T_g.

Results and discussion

General trends

Figure 3a and b show the evolution of storage modulus, E', over the whole temperature range, for pure PMMA and for PMMA/(MTOS or MDCS) silica networks, respectively. Each curve demonstrates clearly the occurrence of the α relaxation in the high-temperature range. In addition to the α damping process, the loss modulus E'' curves reveal (Fig. 4a and b) the occurrence of a broad β relaxation in the low-temperature range. The experimental results are analyzed below in discussing successively these two temperature ranges.

Analysis of the high-temperature range

Over this temperature range, we will examine successively: (a) the main relaxation temperature, T_α, and the

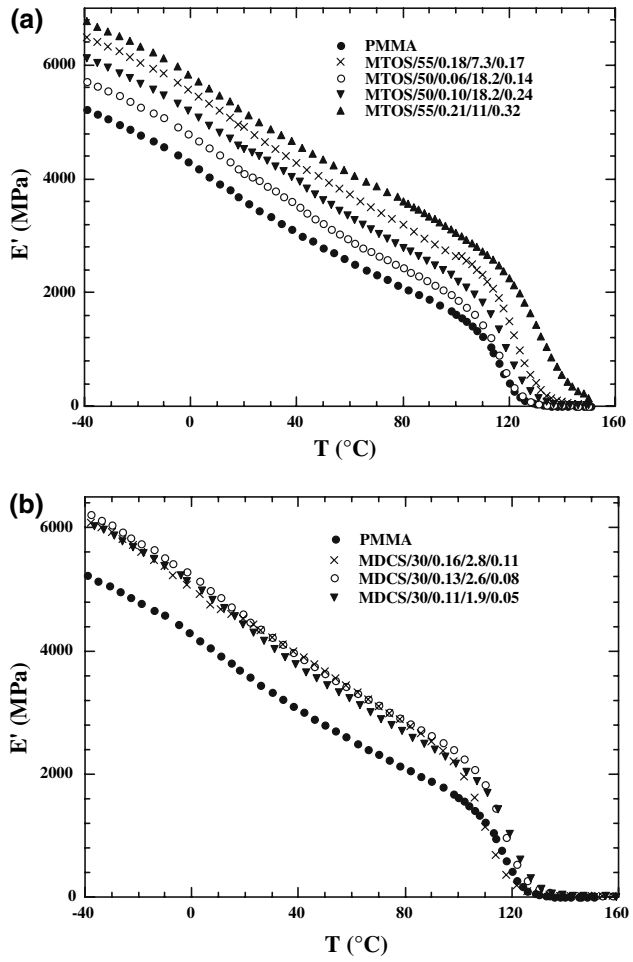

Fig. 3 Storage modulus E'_c at 1 Hz vs. temperature for: (**a**) pure PMMA and MTOS grafted nanosilica systems; (**b**) pure PMMA and MDCS grafted nanosilica systems

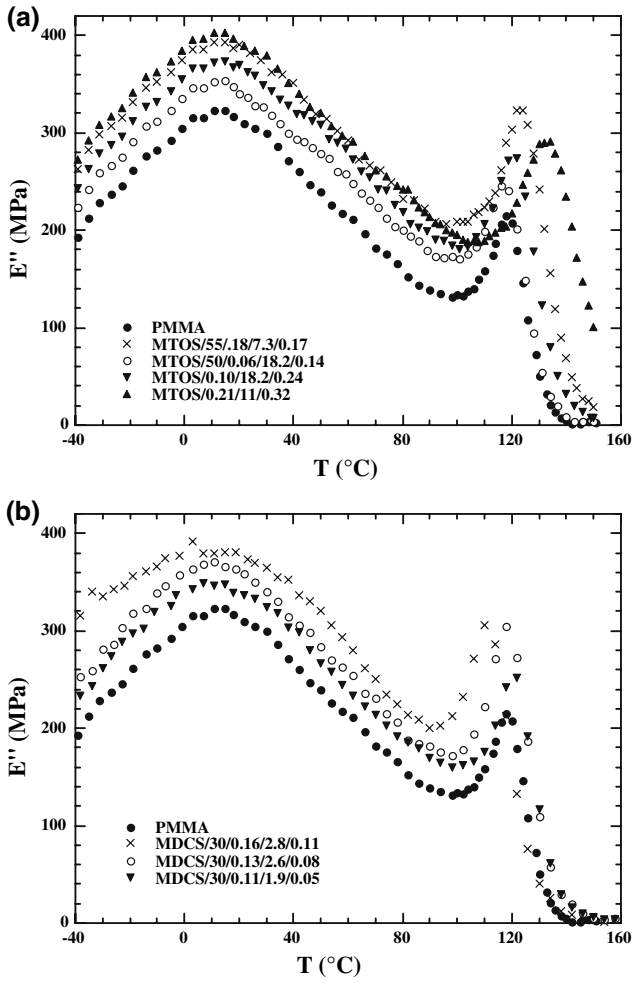

Fig. 4 Loss modulus E''_c at 1 Hz vs. temperature for: (**a**) pure PMMA and MTOS grafted nanosilica systems; (**b**) pure PMMA and MDCS grafted nanosilica systems

α peak width, (b) the glassy modulus, and (c) the rubbery modulus at $T = T_\alpha + 50$ K.

Main relaxation α

Table 1 compares, for all tested materials, the T_α values to the T_g values previously determined [9] at the inflexion point of the DSC thermograms recorded at 10 °C mn^{-1}. It turns out that thermal and mechanical expressions of the glass transition covered the same temperature range. For MTOS networks, Fig. 5 shows the correlation holding between T_α and ξ_D, which is analogous to that previously established between T_g and ξ_D [9]. In other words, Tα increases with increasing cross-link density; this effect can be easily explained by the reduction in chain mobility associated to the presence of the cross-links. On the other hand, it is surprising noting an opposite effect in the MDCS grafting case. In particular, the network referred as ''MDCS/30/0.16/2.8/0.11,'' exhibits a T_α value significantly lower than pure PMMA (111 °C instead of 118 °C). Such an effect cannot be attributed to experimental errors, as the DSC measurements lead to the same trends [9]. We think rather that this experimental observation would give evidence for a plasticization phenomenon around the particles, in connection to the presence of unreacted short chains. Let us recall, indeed, that the synthesis of defect-free networks has proven to be more difficult to achieve in the MDCS series than in the MTOS series [9] and that less drastic conditions on the amount of sol fraction have been retained for the MDCS samples (see experimental section).

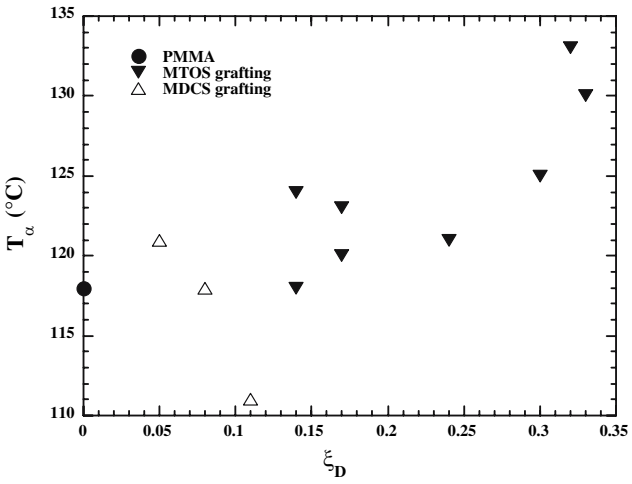

Fig. 5 Main mechanical relaxation temperature T_α vs. ξ_D for the grafted nanosilica systems

In agreement with the earlier DSC observations, a slight broadening of the α peak is observed. As tentatively proposed in reference [9], this effect is probably due to a certain distribution of the cross-link densities within the networks. By the way, one should notice that the change in shape of the β damping peak as a function of Φ prevents any quantitative comparison of the E'' values to be made from one sample to the other.

Glassy modulus

Figure 3a and b also put into evidence that, at any given temperature, all composites have a higher glassy modulus than the pure PMMA. Presence of silica which is characterized by a much higher modulus than the glassy polymer (typically 60 GPa at ambient temperature) is primarily suspected to be responsible for this feature. However, one should also remember that T_α increases with increasing silica content (as shown in the above section) and that, in turn, the larger the gap $(T - T_\alpha)$ between T_α and the testing temperature T, the higher the glassy modulus is. Therefore, with the aim of breaking free from the latter effect, we propose to compare the storage moduli E' of different samples at same gap $(T - T_\alpha)$. As shown in Fig. 6a and b the plots of E' versus $(T - T_\alpha)$ confirm unambiguously that E' values increase with increasing volume fraction of silica ϕ. Quantitatively, these E' experimental values for composites have to be compared with those calculated from theoretical models which only need knowing some characteristics (elastic modulus, Poisson coefficient, volume fraction, morphology) of each component. Among the numerous theoretical models available in the literature, two simple models (Kerner and Christensen & Lo) are considered, which are based on quite different approaches.

The Kerner model [18–20], based on a geometric approach, is suitable for composites including spherical particles at low volume fraction only. Moreover, the particle-matrix adhesion is assumed to be perfect in order to exclude any debonding effect. In Kerner's approach, the elementary representative volume is a spherical inclusion covered by a shell of matrix. The calculation is performed, assuming linear elasticity, for hydrostatic or tensile test conditions. In the case of particles presenting a much higher modulus than the matrix, a simple relation holds for the composite Young's modulus E_c:

$$\frac{E_c}{E} = 1 + \left[\frac{15(1-\nu_m)}{8-10\nu_m}\right]\left[\frac{\Phi}{1-\Phi}\right] \quad (1)$$

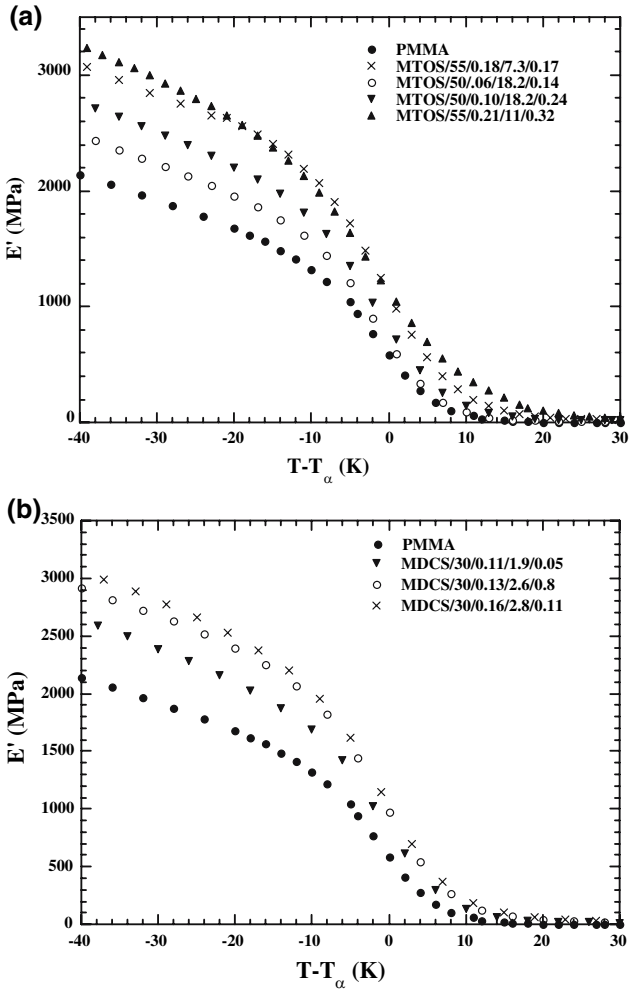

Fig. 6 Storage modulus E_c' at 1 Hz vs. the departure $(T–T_\alpha)$ from T_α in the glassy state for: (**a**) pure PMMA and MTOS grafted nanosilica systems; (**b**) pure PMMA and MDCS grafted nanosilica systems

In Eq. 1, E_m and ν_m represent the Young modulus and the Poisson coefficient of the matrix, respectively. It is worth noticing that all the hypotheses attached to Kerner's model are fulfilled by all the samples under study here.

The Christensen & Lo model [21] is more recent and based on an auto-coherent approach. It is a three-phase model which considers an elementary representative volume, similar to that introduced by Kerner, placed inside a third virtual phase of infinite dimensions called ''equivalent homogeneous surroundings.'' This third phase exhibits analogous properties to those of the global composite that we aim to calculate. In that case, the composite shear modulus G_c can be obtained by solving the quadratic equation:

$$A\left(\frac{G_c}{G_m}\right)^2 + B\left(\frac{G_c}{G_m}\right) + C = 0. \quad (2)$$

The coefficients A, B and C can be calculated [19] from the volume fraction of filler, Φ, and the shear moduli, G_c and G_p, and the Poisson's ratio, ν_m and ν_p, of the matrix and the filler, respectively:

$$\begin{aligned}
A =& 8\left(\frac{G_p}{G_m}-1\right)(4-5\nu_m)\eta_1\Phi_v^{10/3} \\
&-2\left[63\left(\frac{G_p}{G_m}-1\right)\eta_2+2\eta_1\eta_3\right]\Phi_v^{7/3} \\
&+252\left(\frac{G_p}{G_m}-1\right)\eta_2\Phi_v^{5/3} \\
&-50\left(\frac{G}{G_m}-1\right)(7-12\nu_m+8\nu^2)\eta_2\Phi_v+4(7-10\nu_m)\eta_2\eta_3 \\
B =& -4\left(\frac{G_p}{G_m}-1\right)(1-5\nu_m)\eta_1\Phi_v^{10/3} \\
&+4\left[63\left(\frac{G_p}{G_m}-1\right)\eta_2+2\eta_1\eta_3\right]\Phi_v^{7/3} \\
&-504\left(\frac{G_p}{G_m}-1\right)\eta_2\Phi_v^{5/3} \\
&+150\left(\frac{G}{G_m}-1\right)(3-\nu_m)\nu_m\eta_2\Phi_v+3(15\nu_m-7)\eta_2\eta_3 \\
C =& 4\left(\frac{G_p}{G_m}-1\right)(5\nu_m-7)\eta_1\Phi_v^{10/3} \\
&-2\left[63\left(\frac{G_p}{G_m}-1\right)\eta_2+2\eta_1\eta_3\right]\Phi_v^{7/3} \\
&+252\left(\frac{G_p}{G_m}-1\right)\eta_2\Phi_v^{5/3} \\
&+25\left(\frac{G}{G_m}-1\right)(\nu_m^2-7)\eta_2\Phi_v-(7+5\nu_m)\eta_2\eta_3
\end{aligned}$$

with

$$\begin{aligned}
\eta_1 &= (49-50\nu_m\nu_p)\left(\frac{G_p}{G_m}-1\right)+35\frac{G_p}{G_m}(\nu_p-2\nu) \\
&\quad +35(2\nu_p-\nu_m) \\
\eta_2 &= 5\nu_p\left(\frac{G}{G_m}-8\right)+7\left(\frac{G}{G_m}+4\right) \\
\eta_3 &= \frac{G_p}{G_m}(8-10\nu)+(7-5\nu_m)
\end{aligned}$$

Due to the low Φ values in the systems of this study, it is assumed that the composite Poisson coefficient does not differ significantly from that of the matrix; therefore, the Young's moduli E_c and E_m, can be considered in Eq. 2 in place of the relevant shear moduli.

In Fig. 7a and b, the experimental values, obtained for the storage modulus E_c' of composite, are compared to the theoretical values at three temperatures, namely $(T_\alpha–40\ K)$, $(T_\alpha–20\ K)$ and $(T_\alpha–10\ K)$. These

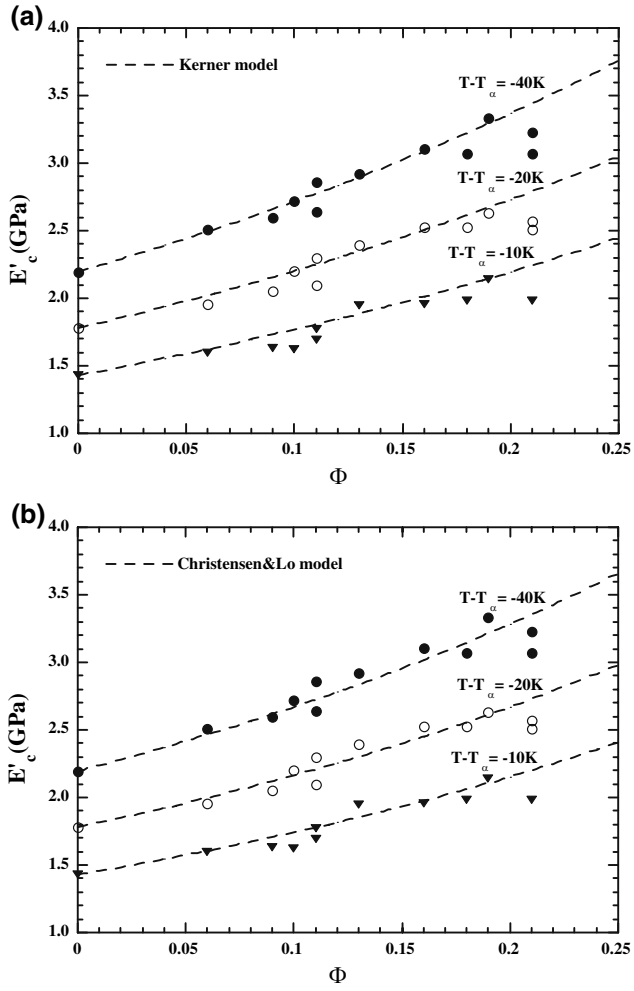

Fig. 7 Fit of the experimental storage modulus E_c' values, measured in the glass transition region by two theoretical approaches: (**a**) Kerner's model; (**b**) Christensen & Lo's model

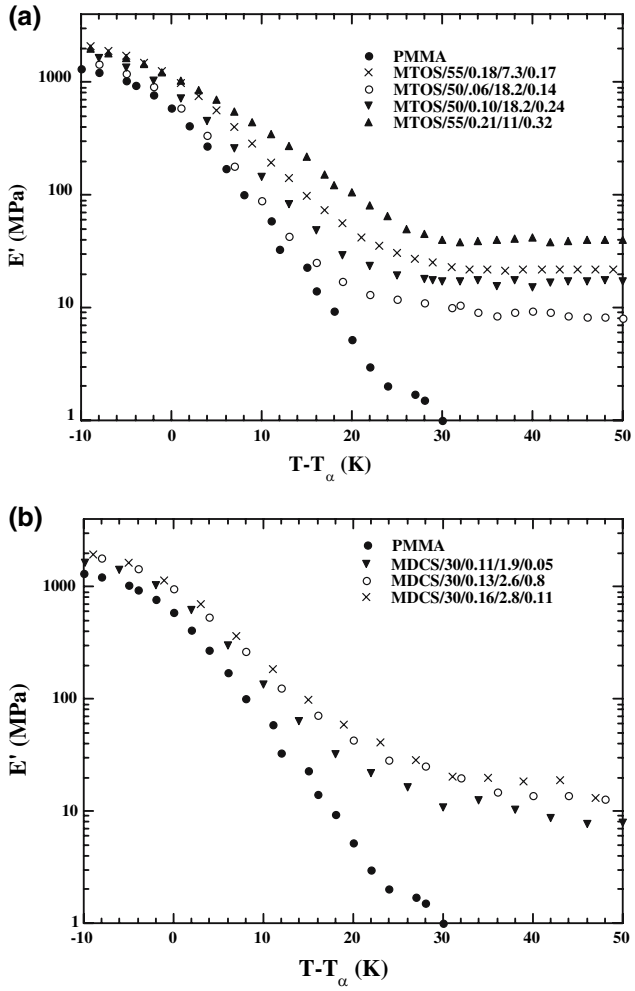

Fig. 8 Storage modulus E_c' at 1 Hz vs. the departure (T–T_α) from T_α, in the rubbery plateau region, for: (**a**) pure PMMA and MTOS grafted nanosilica systems; (**b**) pure PMMA and MDCS grafted nanosilica systems

theoretical values have been calculated in taking in account the variation of the matrix shear modulus E_m with the temperature. In fact, the calculation did not need adjustable parameter, we had only assumed that $\nu_m = \nu_p = 0.33$. It can be seen that the two theoretical approaches, in the temperature range of α relaxation, allow to correctly reproduce the experimental dependence of E_c' on ϕ; in this case, the two models work likewise.

Rubbery modulus

Above T_α, a rubbery plateau, which does not exist for pure PMMA, shows up for the all silica-filled PMMA samples (Fig. 8a, b). This permanent plateau is correlated to the formation of a chemical three-dimensional network during the composite synthesis. A possible explanation for the absence of any plateau in pure PMMA would be the presence of numerous short chains whose early flow, just above T_α, cuts off the transient plateau associated to the entangled long chains. Moreover, it can be noticed that the rubbery modulus E_c' varies as a function of filler content. Such a variation for E_c' can arise from two causes, namely: (1) the effect on modulus of any changes in filler volume fraction Φ, as discussed in the above paragraph; and also (2) the change in matrix modulus as the result of variations in cross-link density. A two-step methodology has been followed to give an account for these two contributions.

In a first step, the values of matrix modulus, E_m', were calculated knowing the experimental values of composite modulus, E_c', and the volume fraction of filler. For the sake of consistency with the glassy modulus considerations reported above, Kerner's equation was used at $T = T_\alpha + 50$ K, in the form:

Table 2 Values of experimental rubbery composite modulus E_c' and of matrix modulus E_m' calculated from Kerner and Guth & Gold model, respectively

Sample reference	E_c' Experimental at T_α + 30 K	E_m' Calculated at T_α + 30 K from Kerner's model	E_m' Calculated at T_α + 30 K from Guth & Gold's model
PMMA	1.6		
MTOS/30/0.11/7/0.17	15	11.5	10.4
MTOS/50/0.06/18.2/0.14	8	6.9	6.7
MTOS/50/0.10/18.2/0.24	17.5	13.7	12.6
MTOS/55/0.18/7.3/0.17	22	14.2	11.5
MTOS/55/0.21/11/0.32	40	24	18.6
MTOS/100/0.21/18.5/0.30	27	16.2	12.6
MTOS/100/0.09/23.5/0.14	11	8.8	8.2
MTOS/100/0.19/23.5/0.33	37	23.3	18.7
MDCS/30/0.16/2.8/0.11	11	7.4	6.1
MDCS/30/0.11/1.9/0.05	4	3	2.7
MDCS/30/0.13/2.6/0.08	8	5.8	5

$$E'_m = \frac{E_c}{\left(1 + \frac{5}{2}\left(\frac{\Phi}{1-\Phi}\right)\right)} \quad (3)$$

which is deduced from Eq. 1 assuming ν_m equal to 0.5 in the rubbery state.

As a tribute to the usual habits in the studies on filled elastomers, E_m' was also calculated by using the well-known Guth & Gold equation [22] which takes into account the pair interaction between particles:

$$E'_m = \frac{E'_c}{1 + 2.5\Phi + 14.1\Phi^2} \quad (4)$$

As shown in Table 2, rather slight differences result from two calculations. As an important result, the E_m' values are not the same (within the error bars on the calculations) for the different samples under study.

Then, the second step is to show that the E_m' values actually depend on the cross-link density. To this end, E_m' was plotted as a function of the parameter ξ_D (Fig. 9a, b), and an unambiguous linear relationship was found between these two quantities. By the way, one may notice that the Guth & Gold approach gives an extrapolated E_m' value at $\xi_D = 0$ in better accordance to the value of 1.6 MPa which corresponds to the rubbery modulus of pure PMMA extracted from rheological measurements.

In conclusion, it turns out that the increase in rubbery modulus with increasing Φ is actually the result of two additive contributions, a first one due to the higher modulus of silica particles on the one hand, the other due to the increase on cross-link density on the other hand.

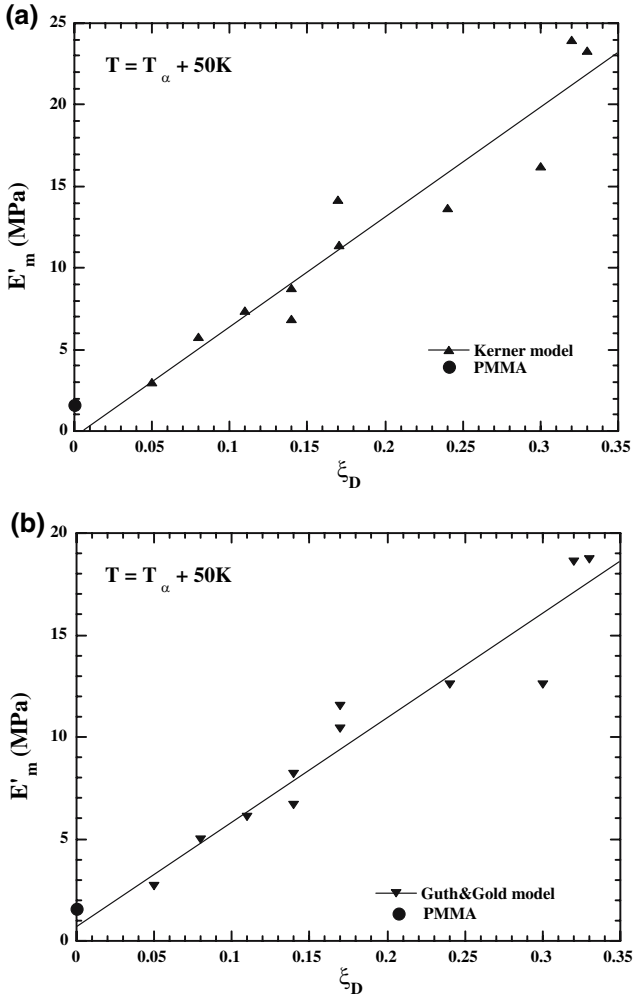

Fig. 9 Calculated storage modulus E_m' of matrix versus ξ_D at T_α + 50 K: (**a**) Kerner's model; (**b**) Guth & Gold's model

Analysis of the low-temperature range

Now, let us focus our attention on the β secondary relaxation domain, which spreads from –40 °C to 80 °C irrespectively of the filler content. By contrast to the situation encountered in the previous section, this feature means that considerations based on the E'' values are suitable over this temperature range. Figure 10a and b

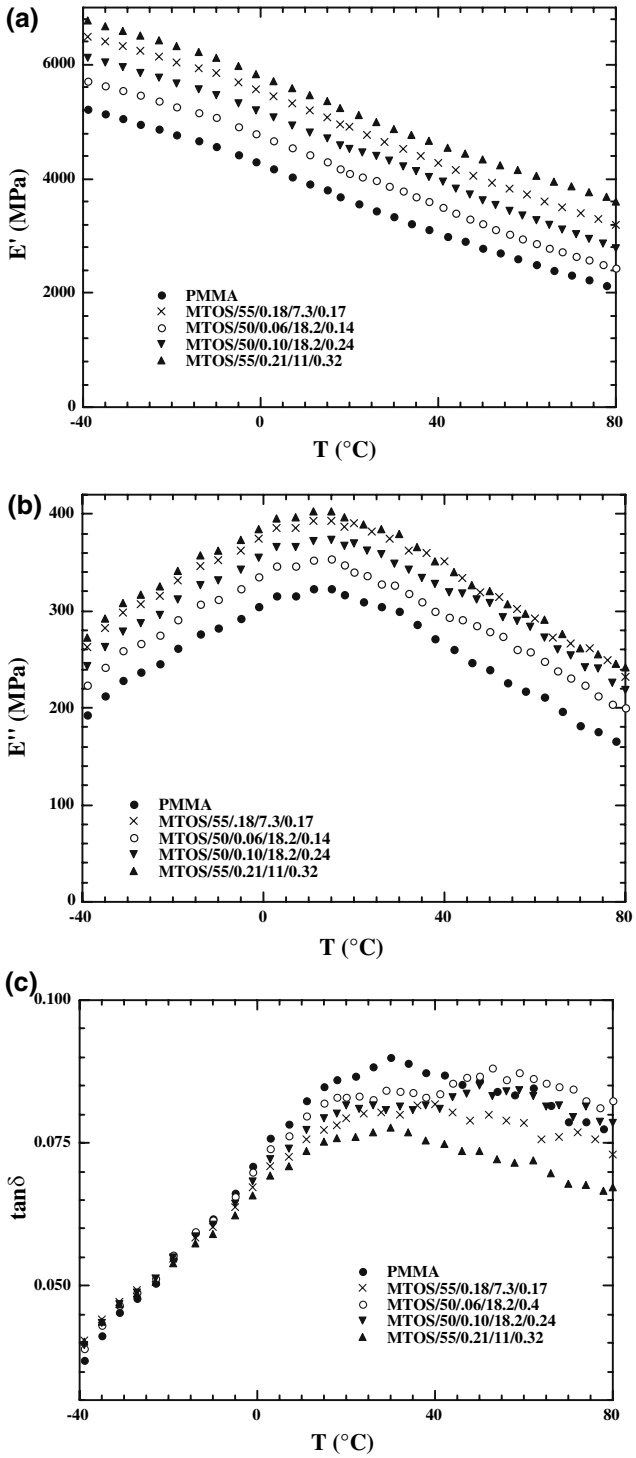

Fig. 10 Temperature dependence of the viscoelastic characteristics at 1 Hz in the *beta* relaxation region: (**a**) E'; (**b**) E''; (**c**) tanδ

demonstrate, for all composites, an increase in both storage and loss modulus as compared to pure PMMA. As for E' over the temperature range of α relaxation, the values are increasing with the volume fraction Φ of nanoparticles. On the other hand, Fig. 10c gives evidence for a slight decrease of $\tan\delta = \frac{E''}{E'}$ with increasing Φ; this result means that the rise of storage modulus is the prevailing effect. As for the α relaxation region, the Kerner's model has been used for reproducing the variation of E_c' as a function of Φ at various temperatures. Figure 11a shows that experimental and theoretical values are not in good accordance over the whole filler volume fraction range; in fact, we observe, for high Φ values ($\Phi > 0.12$), a discordance which increases as the temperature is decreasing. At the moment, we have no explanation on the fact that the Kerner's model works better in the α relaxation domain. The analysis of E''_c variation as a function of Φ needs a more sophisticated treatment because two competing effects contribute to the observed results.

First, the existence of debonding at the filler–matrix interface (cavitation) can involve an increase in loss energy. In the case of our materials, a good adhesion exists between fillers and polymer chains, which renders dubious this cavitation effect.

Secondly, the β damping is only associated to local movements of the ester group [23, 24] belonging to MMA units; so, we should take into account the dilution effect marked by the decrease of the number of MMA monomers in the composite volume unit when Φ is increasing. Some studies performed in our Laboratory [25–27] have shown that such a dilution effect can be analyzed satisfactorily by adding up the loss compliances corrected by the volume fraction of each component. As no loss energy can be imputed to the filler, this treatment allows calculation of the effective compliance J''_{eff} of the matrix by using the following equation:

$$J''_{\text{eff}} = \frac{J''_c}{1-\Phi} \tag{5}$$

where J''_c is derived from the experimental E_c' and E''_c values obtained for the composite according to the equation:

$$J''_c = \frac{E''_c}{E'^2_c + E''^2_c} \tag{6}$$

Finally, the effective loss modulus E''_{eff} of the matrix can be evaluated by combining the Eqs. 5 and 6:

$$E''_{\text{eff}} = \frac{\left(E'^2_c + E''^2_c\right) \times J''_c}{1-\Phi}. \tag{7}$$

Figure 11b shows that the Kerner's model reproduces correctly the evolution of loss modulus in the β relaxation region.

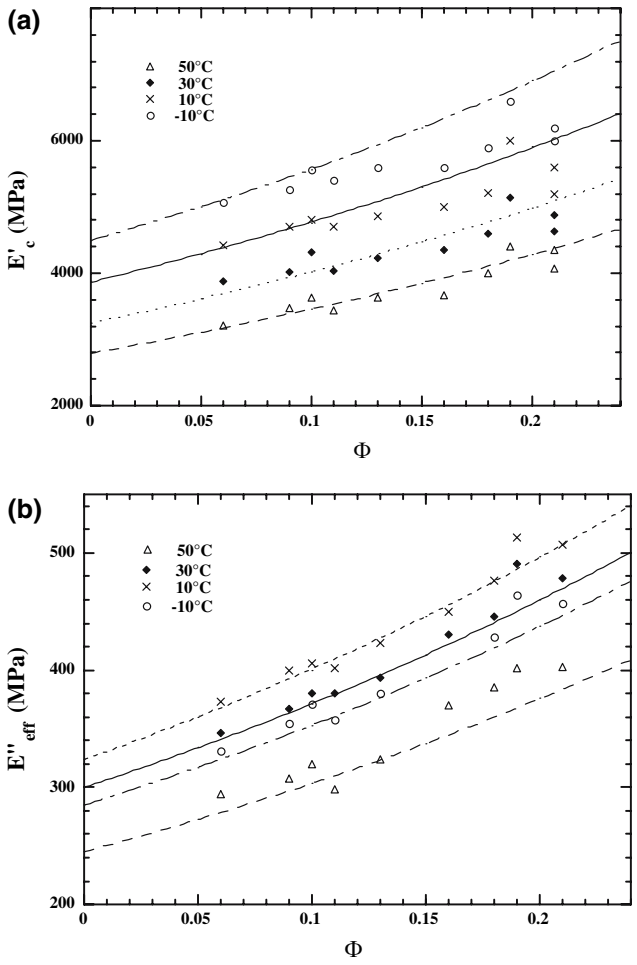

Fig. 11 Fit of moduli by to Kerner's model in the β relaxation region: (**a**) storage modulus E_c'; (**b**) effective loss modulus E''_{eff}

Conclusions

Mechanic dynamical measurements performed on nanosilica filled PMMA have revealed that the different temperature regions (β relaxation, α relaxation and rubbery plateau) deserve to be analyzed differently.

In the α relaxation region, analysis of the loss peak data leads to conclusions analogous to those deduced from DSC investigations [9]: the glass transition temperature slightly increases with the parameter ξ_D which properly accounts for the cross-link density; in parallel to this effect, an enlargement of the glass transition range is observed. Just below T_α, the observed increase in storage modulus with the volume fraction Φ of filler can be fairly reproduced by two different theoretical approaches, namely the Kerner and Christensen & Lo models.

In the rubbery plateau region ($T > T_\alpha + 30$ K), the increase of the rubbery modulus with Φ has been analyzed by means of the Kerner or Guth & Gold models. These two models lead to the same conclusion: the cross-links attached to the filler contribute to the increase in matrix storage modulus.

Inspection of the low-temperature range, governed by the β relaxation processes, puts into evidence that the storage and loss modulus vary differently as a function of Φ. While the storage modulus roughly follows Kerner predictions, the loss modulus behavior needs to take into account a dilution effect of β movements due to the fact that no damping process is associated to the fillers. Thereby, we observe a decrease in loss angle as Φ increases.

Thus, thanks to the synthesis of numerous hybrid networks of well-defined architecture, a comprehensible analysis of the viscoelastic properties of these new materials has been carried out. Their viscoplastic properties and fracture behavior have been also analyzed; their presentation and analysis will be the matter of a forthcoming publication.

Acknowledgements The support of the French Ministry of Research and Technology through the PhD grant provided to one of us (M.M) is gratefully acknowledged.

References

1. Alexandre M, Dubois P (2000) Mater Sci Eng 28:1
2. Ruan WH, Zhang MQ, Rong MZ, Friedrich K (2004) J Mater Sci 39:3475
3. Ruan WH, Zhang MQ, Rong MZ, Friedrich K (2003) Polym Eng Sci 43:490
4. Chang J-H, An YU, Sur GS (2003) J Polym Sci: Part B: Polym Phys 41 (2003) 94
5. Yano K, Usuki A, Osaka A (1997) J Polym Sci: Part A: Polym Chem 35:2289
6. Kashiwagi T, Grulke E, Hilding J, Groth K, Harris R, Butler K, Shields J, Kharchenko S, Douglas J (2004) Polymer 45:4227
7. Qin H, Su Q, Zhang S, Zhao B, Yang M (2003) Polymer 44:7533
8. Xu Y, Brittain WJ, Xue C, Eby RB (2004) Polymer 45:3735
9. Mauger M, Dubault A, Halary JL (2004) Polym Int 53:378
10. Li Y, Zhao B, Xie S, Zhang S (2003) Polym Int 52:892
11. Moussaif N, Groeninckx G (2003) Polymer 44:7899
12. Ash BJ, Schadler S, Sielgel RW (2002) Mater Lett 55:83
13. Ash BJ, Sielgel RW, Schadler S (2004) J Polym Sci: Part B: Polym Phys 42:4371
14. Sunkara HB, Jethmalani JM, Ford WT (1994) Chem Mater 6:362
15. Jethmalani JM, Ford WT (1996) Chem Mater 8:2138
16. Jethmalani JM, Sunkara HB, Ford WT (1997) Langmuir 13:2633

17. Jethmalani JM, Ford WT (1997) Langmuir 13:3338
18. Kerner EH (1956) Proc Phys Soc 69B:808
19. Nielsen LE (1966) J Appl Polym Sci 10:97
20. Ramsteiner R, Theysohn R (1984) Composites 15:121
21. Christensen RM, Lo KH (1979) J Mech Phys Solids 27:315
22. Guth E, Gold O (1938) Phys Rev 53:322
23. Tordjeman P (1992) Thesis, University Pierre and Marie Curie, Paris
24. Tézé L (1995) Thesis, University Pierre and Marie Curie, Paris
25. Heux L, Lauprêtre F, Halary JL, Monnerie L (1998) Polymer 39:1269
26. Tézé L, Halary JL, Monnerie L, Canova L (1999) Polymer 40:971
27. Dubault A, Bokobza L, Gandin E, Halary JL (2003) Polym Int 52:1108